The Thermohaline Circulation and Vertical Mixing: Does Weaker Density Stratification Give Stronger Overturning?

JOHAN NILSSON AND GÖRAN BROSTRÖM

Department of Meteorology, Stockholm University, Stockholm, Sweden

GÖSTA WALIN

Department of Oceanography, Göteborg University, Göteborg, Sweden

(Manuscript received 8 August 2002, in final form 2 June 2003)

ABSTRACT

The possibility that a decreased equator-to-Pole surface density difference could imply stronger rather than weaker thermohaline circulation (THC) is explored theoretically as well as with the aid of numerical simulations. The idea builds on the classical thermocline scaling, stating that the THC should increase with density difference as well as with vertical diffusivity. To explore possible changes in vertical diffusivity that would follow a change in the oceanic density difference, simple models of internal wave mixing are considered. For reasonable assumptions concerning the energy supply to vertical mixing, the overall diffusivity tends to increase with decreasing density difference. This enhancement of the vertical diffusivity acts to deepen the thermocline, an effect that can cause the THC to amplify despite that the surface density difference is reduced. This remarkable state of affairs is illustrated with simulations from a one-hemisphere ocean circulation model. In the simulations, two stratification-dependent diffusivity representations are investigated, which both imply that a weaker density difference will be associated with a stronger THC. The more common mixing representation, where the diffusivity is taken to be fixed, yields the opposite and well-known result: a weaker density difference will be associated with a weaker THC.

1. Introduction

The relation between the strength of the thermohaline circulation (THC) and the equator-to-Pole density difference must be considered as one of the fundamental questions in oceanography. Because the THC carries huge amounts of heat poleward, this question is also of importance in the context of climate (e.g., Broecker 1997). During the past two decades a large number of investigations have contributed to our understanding of how the THC operates (see Marotzke 2000; Rahmstorf 2000, for a current perspective). Presently, the general view is that the rate-limiting THC branch is the upwelling of dense water, rather than the high-latitude production and sinking of dense water (e.g., Marotzke and Scott 1999; Huang 1999).

In the present ocean, two different processes drive upwelling of dense deep water masses: first, small-scale vertical mixing in the interior ocean (Munk and Wunsch 1998), which drives upwelling in the low latitudes, and, second, wind-forced upwelling in the Southern Ocean (Toggweiler and Samuels 1995) where the surface Ekman drift carries cold water equatorward. The relative contributions from Southern Ocean winds and small-scale vertical mixing to the present global upwelling are rather poorly constrained. This state of affairs partly reflects an uncertainty regarding the strength of the small-scale mixing in the World Ocean (Toole and McDougall 2001). However, it has been argued (e.g., Webb and Suginohara 2001) that as much as one-half of the deep water formed in the North Atlantic returns to surface in the Southern Ocean.

The present investigation focuses on the THC component that wells up in the stratified low-latitude ocean. Conceptually, we may think of this THC mode as an overturning circulation with narrow sinking in high latitudes and broad upwelling in low latitudes. While it is questionable if the real THC can be disentangled in one Pole-to-Pole and one equator-to-Pole component, the latter THC mode has been extensively studied in single-hemisphere ocean models (see Park and Bryan 2000, for an overview). In this geometry, a straightforward scaling argument suggests that the THC strength (say, ψ) obeys (e.g., Welander 1986)

$$\psi \sim \Delta\rho^{1/3}\kappa^{2/3},$$

where $\Delta\rho$ is the equator-to-Pole density difference and

Corresponding author address: Johan Nilsson, Department of Meteorology, Stockholm University, 106 91 Stockholm, Sweden.
E-mail: nilsson@misu.su.se

κ is the vertical diffusivity. If κ is fixed, the THC strength obviously increases with density difference.

In the ocean, however, the vertical diffusivity presumably depends on the vertical density stratification, which in turn is coupled to the equator-to-Pole density difference. Accordingly, a change of $\Delta\rho$ will imply also a change of κ. Recently, Nilsson and Walin (2001) investigated this issue with the aid of an analytical two-layer model of the THC. Their analysis illustrates that, if the vertical diffusivity decreases with increasing stratification (a physically motivated feature), the THC may, in fact, slow down in response to an increased equator-to-Pole density difference. This result is contrary to the established view, which is based on the assumption that the vertical diffusivity is independent of the stratification. The fact that the representation of vertical mixing can change the qualitative behavior of the THC has also been pointed out by Lyle (1997) and Huang (1999).

The unexpected and somewhat counterintuitive result—that a stronger surface density difference can yield a weaker overturning—can be illuminated as follows. To lift a parcel of water from the deep ocean (adiabatically through the stratification) to the surface requires work as the potential energy of the parcel increases. In the low-latitude upwelling branch, this work is performed by small-scale vertical mixing, which heats the rising cold water at a rate that keeps its buoyancy neutral. Energetically, the small-scale vertical mixing and its associated production of potential energy should thus be viewed as the driving agent of the upwelling (Weyl 1968; Munk and Wunsch 1998). Accordingly, if the energy supply (chiefly from winds and tides) to the small-scale vertical mixing is fixed, we intuitively expect that a weaker vertical density contrast would allow for a stronger upwelling.

The main objective of the present study is to further explore the intriguing question raised by Nilsson and Walin (2001): Can a reduced surface density contrast result in a stronger THC? We consider a one-hemisphere ocean basin and investigate how the representation of vertical mixing affects the dynamics of the THC. For this purpose, we make use of scaling arguments as well as simulations with an ocean general circulation model. Our main results are summarized in Figs. 3 and 4. In the concluding section, we discuss the relevance of the present ''one hemisphere'' result for the real THC.

2. Vertical mixing and the strength of the THC

a. Scale analysis

To investigate how the features of small-scale mixing affect the THC dynamics, we revisit classical thermocline scaling arguments; see e.g., Welander (1986) and Park and Bryan (2000). We consider the circulation in a one-hemisphere basin and characterize the oceanic density structure with two variables: the equator-to-Pole density difference ($\Delta\rho$) and the thermocline depth (H), measuring the thickness of the upper stratified ocean above the deep water. We consider $\Delta\rho$ as an imposed quantity, while H and the THC strength are determined by the dynamics of the system. Note that in the present-day ocean, also the vertical density difference is proportional to $\Delta\rho$ (see Fig. 2 for an illustration of an oceanlike density distribution). For the sake of simplicity, we ignore interaction between the THC and the wind-driven gyre circulation, an issue that has been discussed in detail by Samelson and Vallis (1997) and Vallis (2000).

In the scale analysis, the following dynamical assumptions are made:

1) continuity of mass;
2) the flow is in hydrostatic and geostrophic balance, which yields the thermal wind relation

$$\frac{\partial v}{\partial z} = -\frac{g}{f\rho_0}\frac{\partial \rho}{\partial x}, \tag{1}$$

   where v is the meridional velocity, z is the vertical coordinate, g is the acceleration of gravity, f is the Coriolis parameter, x is the east–west coordinate, ρ is the density, and ρ_0 is the mean density; and
3) the stratification and the associated diapycnal flow are governed by an advective–diffusive balance

$$w\frac{\partial \rho}{\partial z} = \frac{\partial}{\partial z}\left(\kappa\frac{\partial \rho}{\partial z}\right), \tag{2}$$

   where w is the vertical velocity and κ is the vertical diffusivity.

We now perform a scale analysis to obtain the dependence of the thermocline depth and the overturning strength on the imposed equator-to-Pole density difference. The presentation essentially follows that of Nilsson and Walin (2001). First, we estimate the strength of the horizontal THC branch. By assuming that the meridional and the zonal density gradients are proportional, Eq. (1) suggests that the poleward volume transport should be proportional to

$$\psi \sim \Delta\rho H^2 g/(\rho_0 f). \tag{3}$$

In addition to its physical basis in the thermal wind relation, this straightforward relation is supported by the results of several numerical modeling studies (e.g., Marotzke 1997; Park and Bryan 2000); it is relevant, however, to underline that Eq. (3) requires that the north–south density gradients are linked to the east–west gradients.

Next, we obtain an independent estimate of the THC strength in the upwelling branch with aid of the advective–diffusive balance equation [Eq. (2)], which it proves convenient to reformulate as

TABLE 1. Summary of scaling results for different representations of κ; see Eqs. (8)–(10) and section 2b. (The cases named A, B, and C are explored in the numerical simulations.) The scale dependence of dissipation, diffusivity, thermocline depth, and overturning strength on the equator-to-Pole density difference is given. Note that dissipation here refers to the implied sink of turbulent energy associated with the vertical mixing; see Eq. (16).

λ (case)	Dissipation	Diffusivity	Thermocline	Circulation
$\lambda = 1/3$ (A)	$\mathcal{E} \sim \Delta\rho$	$\kappa \sim$ const	$H \sim \Delta\rho^{-1/3}$	$\psi \sim \Delta\rho^{1/3}$
$\lambda = 1/7$	$\mathcal{E} \sim \Delta\rho^{5/7}$	$\kappa \sim \Delta\rho^{-2/7}$	$H \sim \Delta\rho^{-3/7}$	$\psi \sim \Delta\rho^{1/7}$
$\lambda = 1/11$	$\mathcal{E} \sim \Delta\rho^{7/11}$	$\kappa \sim \Delta\rho^{-4/11}$	$H \sim \Delta\rho^{-5/11}$	$\psi \sim \Delta\rho^{1/11}$
$\lambda = -1/5$ (B)	$\mathcal{E} \sim \Delta\rho^{1/5}$	$\kappa \sim \Delta\rho^{-4/5}$	$H \sim \Delta\rho^{-3/5}$	$\psi \sim \Delta\rho^{-1/5}$
$\lambda = -1/3$ (C)	$\mathcal{E} =$ const	$\kappa \sim \Delta\rho^{-1}$	$H \sim \Delta\rho^{-2/3}$	$\psi \sim \Delta\rho^{-1/3}$

$$wN^2 = \frac{\partial \kappa N^2}{\partial z}, \tag{4}$$

where N, the buoyancy frequency, is defined by

$$N = \sqrt{-\frac{g}{\rho_0}\frac{\partial \rho}{\partial z}}. \tag{5}$$

If the basin area is A, the strength of the upwelling can be estimated as

$$\psi \sim A\kappa H^{-1}. \tag{6}$$

It should be emphasized that this crude estimate is expected to work well only for smooth density profiles characterized by the single depth scale H. Because the strength of diffusivity κ may depend on H and $\Delta\rho$, it is convenient to introduce the following generalized formula

$$\psi \sim \Delta\rho^{-\zeta} H^{-\eta}, \tag{7}$$

where ζ and η are constants that depend on the assumed relation between κ and the stratification.

Last, by requiring the estimates of ψ in the horizontal and the vertical branch to agree (and omitting the constants A, f, g, and ρ_0), we obtain a relation between the imposed equator-to-Pole density difference and the thermocline depth:

$$H \sim \Delta\rho^{(\lambda-1)/2}, \tag{8}$$

where we have introduced

$$\lambda = (\eta - 2\zeta)/(\eta + 2). \tag{9}$$

By substituting Eq. (8) into Eq. (3) we obtain the dependence of the overturning strength on the imposed density difference:

$$\psi \sim \Delta\rho^{\lambda}. \tag{10}$$

To determine the key parameter λ, we must consider how the vertical diffusivity in the interior ocean is coupled to the stratification. This issue is investigated below; the main results are summarized in Table 1, whereas a physical interpretation of the overturning dynamics is postponed to section 2c.

b. The vertical diffusivity in the ocean interior

To begin with, it is worth emphasizing that the problem of parameterizing oceanic vertical mixing is far from fully solved (e.g., Toole and McDougall 2001). In the ocean, the vertical mixing is energetically sustained chiefly by the tides and the winds (Munk and Wunsch 1998), but processes like double-diffusive instabilities (e.g., Toole and McDougall 2001) and tropical cyclones (Nilsson 1996; Emanuel 2001) could potentially also be of importance for the mixing. In terms of a vertical diffusivity, the averaged mixing intensity in the deep ocean is estimated to be on the order of 10^{-4} m^2 s^{-1} (Munk and Wunsch 1998). However, this number is rather poorly constrained (Webb and Suginohara 2001), and observations show that the diffusivity varies strongly geographically. Diffusivities on the order of 10^{-5} m^2 s^{-1} are reported from measurements in the thermocline (and also in many places in the deep ocean), while values 100 times as large are encountered near the bottom in areas with rough topography (Polzin et al. 1995, 1997; Ledwell et al. 2000).

Obviously, it is challenging to develop a mixing representation that captures the complexity of the vertical mixing in the interior ocean. In ocean modeling, this mixing is frequently represented simply by a constant vertical diffusivity, or more generally a fixed vertical profile of κ values (Bryan and Lewis 1979). While this approach yield reasonable simulations of the present-day ocean, it is questionable to assume that the vertical diffusivity would remain unchanged in an ocean with a different stratification (e.g., a situation in which the deep-water production in the North Atlantic is completely terminated).

More physically based parameterization of vertical turbulent diffusivity can be formulated in terms of the turbulent dissipation rate ϵ. Diffusivity is then assumed to be related to dissipation (and the buoyancy frequency N) as (Osborne 1980)

$$\kappa \propto \frac{\epsilon}{N^2}. \tag{11}$$

Below, we will briefly present some theoretical models of internal wave dissipation that have been employed for parameterizing vertical diffusivity in the ocean. The aim is to explore possible relations between κ and the stratification, which here is characterized by the parameters $\Delta\rho$ and H—implying that the buoyancy frequency is estimated as

$$N \sim (\Delta\rho/H)^{1/2}.$$

1) THE LOCAL DISTRIBUTION OF DISSIPATION AND DIFFUSIVITY

Generally, dissipation and diffusivity are assumed to be related to local features of the stratification and to internal wave properties. A school of semianalytical models (e.g., McComas and Müller 1981; Polzin et al. 1995) assumes that the local dissipation is controlled by resonant wave interactions, which transfer energy from large- to small-scale waves. This transfer depends on the stratification and on the internal wave energy per unit area E, as well as on how this energy is distributed over wavenumbers. If internal wave energy is distributed according the Garret–Munk spectrum, the dissipation and diffusivity should obey

$$\epsilon \propto E^2 N^2 \quad \text{and} \quad \kappa \propto E^2. \tag{12a}$$

Note that, in this case, the diffusivity is independent of the local stratification and distributed uniformly through the water column. This particular relation between ϵ and N is supported by numerical wave-interaction simulations (Winters and D'Asaro 1997) and open-ocean microstructure measurements (Polzin et al. 1997).

A somewhat different approach was taken by Gargett and Holloway (1984), who employed scaling arguments to estimate the dissipation rate due to interval wave breakdown. They also found a dependence of the dissipation on the features of the internal wave field. For the Garret–Munk broadband internal wave field, their considerations yield

$$\epsilon \propto EN^{3/2} \quad \text{and} \quad \kappa \propto EN^{-1/2}. \tag{12b}$$

For a monochromatic wave field, on the other hand, the result is

$$\epsilon \propto EN \quad \text{and} \quad \kappa \propto EN^{-1}. \tag{12c}$$

The $\kappa \propto N^{-1}$ relation has, in fact, been inferred from tracer studies in fjords and marginal seas (Gargett 1984; Stigebrandt 1987), but it not clear whether it applies also to the ocean. By assuming that the interval wave energy E is constant, Eqs. (12a–c) immediately yield the following diffusivity (and THC) scaling:

$$\kappa = \text{const}, \qquad (\zeta = 0,\ \eta = 0,\ \lambda = 1/3), \tag{13a}$$

$$\kappa \sim (H/\Delta\rho)^{1/4}, \qquad (\zeta = 1/4,\ \eta = 3/4,\ \lambda = 1/11), \tag{13b}$$

and

$$\kappa \sim (H/\Delta\rho)^{1/2}, \qquad (\zeta = 1/2,\ \eta = 1/2,\ \lambda = -1/5). \tag{13c}$$

The overturning characteristics associated with these diffusivity formulas are presented in Table 1.

2) GLOBAL CONSTRAINTS ON THE VERTICAL DIFFUSIVITY

We emphasize that Eqs. (12a)–(12c) concern the spatial distribution of ϵ and κ given a prescribed internal wave energy level E. The possibility that E depends on some features of the stratification is a different question. To address this issue, we consider the energy balance of the internal wave field. In a steady state, the generation and dissipation of internal wave energy must balance, a condition that can be stated as

$$0 = \mathcal{G} - \mathcal{E}. \tag{14}$$

Here, $\mathcal{G}$ is the rate of internal wave energy supply, and the internal wave dissipation per unit area is defined as

$$\mathcal{E} = \rho_0 \int \langle \epsilon \rangle \, dz, \tag{15}$$

where the integral ranges from the bottom to the surface and angle brackets denote a horizontal average. Further, from the local relation between dissipation and diffusivity (11), it follows that

$$\mathcal{E} \propto \rho_0 \int \langle \kappa N^2 \rangle \, dz, \tag{16}$$

where the right-hand side is the rate of increase in potential energy due to vertical mixing. A qualitative estimate of the integral yields $\mathcal{E} \sim \Delta\rho\kappa$ (recall that $\Delta\rho$ is the vertical density difference). This result, in turn, provides a relation between global diffusivity and dissipation

$$\kappa \sim \frac{\mathcal{E}}{\Delta\rho}. \tag{17}$$

Note that this qualitative relation, which is the global analog of the local relation in Eq. (11), is independent of how the dissipation and the diffusivity are distributed vertically.

To estimate the strength of the diffusivity from Eq. (17), we make the reasonable assumption that the dissipation $\mathcal{E}$ is set by the energy supply to the internal wave field $\mathcal{G}$. Specifically, two different hypotheses concerning the generation of the internal waves are briefly explored:

Pro primo, the internal wave energy supply $\mathcal{G}$ is delivered by the winds. Further, it is assumed that the ocean stratification and the internal wave energy E have minor influence on the energy transfer from winds to internal waves. Putting aside the challenging question of how the wind strength may change in an altered climate, it is here assumed that $\mathcal{E}$ is a constant (controlled by the atmosphere circulation), which implies that

$$\kappa \sim \Delta\rho^{-1}, \qquad (\zeta = 1,\ \eta = 1,\ \lambda = -1/3). \tag{18}$$

This relation is in line with the intuitive notion that a strong stratification acts to suppress turbulence, thereby reducing the vertical diffusivity.

Pro secundo, the internal wave field is energized by the conversion from barotropic to internal tides. This conversion occurs where barotropic tides scatter on rough bottom topography. Following the studies of Bell

(1975) and Llewellyn-Smith and Young (2002), the associated internal wave generation (for a given topography) can be estimated as[1]

$$\mathcal{G} \sim NU_T^2,$$

where U_T is the amplitude of the barotropic tidal flow. Since the bulk of the ocean tidal dissipation is associated with bottom friction in shallow seas (Munk and Wunsch 1998), it is reasonable to assume that U_T is essentially independent of N. This leads to the scaling $\mathcal{G} \sim (\Delta\rho/H)^{1/2}$. Since generation balances dissipation, formula (17) predicts that the diffusivity should obey

$$\kappa \sim (\Delta\rho H)^{-1/2}, \qquad (\zeta = 1/2,\ \eta = 3/2,\ \lambda = 1/7). \tag{19}$$

A somewhat different result follows from the simpler tidal conversion model proposed by Sjöberg and Stigebrandt (1992). They considered internal wave generation at steplike topography and concluded that $\mathcal{G} \sim c_I U_T^2$, where $c_I \sim NH$ is the internal wave speed. This gives the following diffusivity scaling

$$\kappa \sim (H/\Delta\rho)^{1/2}, \qquad (\zeta = 1/2,\ \eta = 1/2,\ \lambda = -1/5). \tag{20}$$

We note that also these two diffusivity estimates predict that a stronger stratification tends to reduce the vertical diffusivity.

3) Relevant special cases

The tentative discussion above suggests a range of possible relations between the stratification and the vertical diffusivity. However, further progress on the physics of the small-scale ocean mixing is required to determine the most relevant parameterization. In particular, the question of how the global dissipation of internal waves would change in a climate with a different ocean stratification remains to be answered. For the sake of simplicity, we will in the following analysis of the THC dynamics consider three of the above mixing parameterizations in closer detail.

Case A: fixed, spatially uniform diffusivity. This corresponds to the internal-wave model in Eq. (12a) with fixed E, implying that

$$\kappa = \text{const}, \qquad E = \text{const}, \quad \text{and} \quad \mathcal{E} \sim \Delta\rho. \tag{21a}$$

Case B: stability-dependent diffusivity $\kappa \sim N^{-1}$. This corresponds to the internal-wave model Eq. (12c) with fixed E, implying that

$$\kappa \sim (H/\Delta\rho)^{1/2}, \qquad E = \text{const}, \quad \text{and}$$
$$\mathcal{E} \sim (\Delta\rho H)^{1/2}. \tag{21b}$$

Case C: Constant global internal-wave dissipation and spatially uniform diffusivity. This corresponds to the internal-wave model Eq. (12a) with fixed global dissipation $\mathcal{E}$, implying that

$$\kappa \sim \Delta\rho^{-1}, \qquad E \sim \Delta\rho^{-1/2}, \quad \text{and} \quad \mathcal{E} = \text{const}. \tag{21c}$$

We emphasize that other parameterizations are plausible. Our particular choice is partly guided by the fact that these cases are straightforward to implement in an ocean circulation model, as will be reported in section 3.

c. Physical interpretation: The thermocline depth adjustment

To illuminate the physics embedded in the general Eqs. (8) and (10), it is instructive to analyze the ramifications of the diffusivity parameterizations described by cases A, B, and C; see above and Table 1. To begin with, case A corresponds to the common assumption of a uniform and fixed vertical diffusivity (i.e., $\zeta = 0$, $\eta = 1$, and $\lambda = 1/3$). This gives the familiar scaling for the advective–diffusive thermocline depth and overturning strength (Welander 1986):

$$H \sim \Delta\rho^{-1/3} \quad \text{and} \quad \psi \sim \Delta\rho^{1/3}. \tag{22a}$$

A fundamental point here is that the overturning strength increases rather weakly with density contrast; the 1/3-power relation implies that a doubling of $\Delta\rho$ yields only about a 25% increase in ψ. The obvious reason is that the thermocline shoals in response to a stronger density difference that, according to the thermal wind scaling in Eq. (3), acts to curtail the overturning.

Consider next case B in which the local diffusivity is inversely proportional to the buoyancy frequency (i.e., $\zeta = 1/2$, $\eta = 1/2$, and $\lambda = -1/5$). It is important to recognize that a stronger density stratification now implies a weaker vertical diffusivity. This feature has a drastic impact on the overturning dynamics, which obeys

$$H \sim \Delta\rho^{-3/5} \quad \text{and} \quad \psi \sim \Delta\rho^{-1/5}. \tag{22b}$$

The decrease in thermocline depth with increasing $\Delta\rho$ is now sharper than when a fixed diffusivity is employed. This can be interpretated as an effect of the reduced vertical diffusivity that follows with a stronger vertical density difference. A remarkable consequence is that the dependence of ψ on $\Delta\rho$ reverses sign: the overturning will decrease rather than increase with stronger imposed density contrast.

This behavior is further accentuated in case C in which the vertical mixing energy $\mathcal{E}$ is fixed (i.e., $\zeta = 1$, $\eta = 1$, and $\lambda = -1/3$). Here the THC dynamics follows

$$H \sim \Delta\rho^{-2/3} \quad \text{and} \quad \psi \sim \Delta\rho^{-1/3}. \tag{22c}$$

Again, we find that the overturning intensifies in re-

[1] Note that N in this formula refers to the near-bottom stratification, whereas in the overturning scaling N characterizes the thermocline. For simplicity, we assume that the near-bottom values of N are proportional to the values in the thermocline; we underline that this is a somewhat questionable assumption.

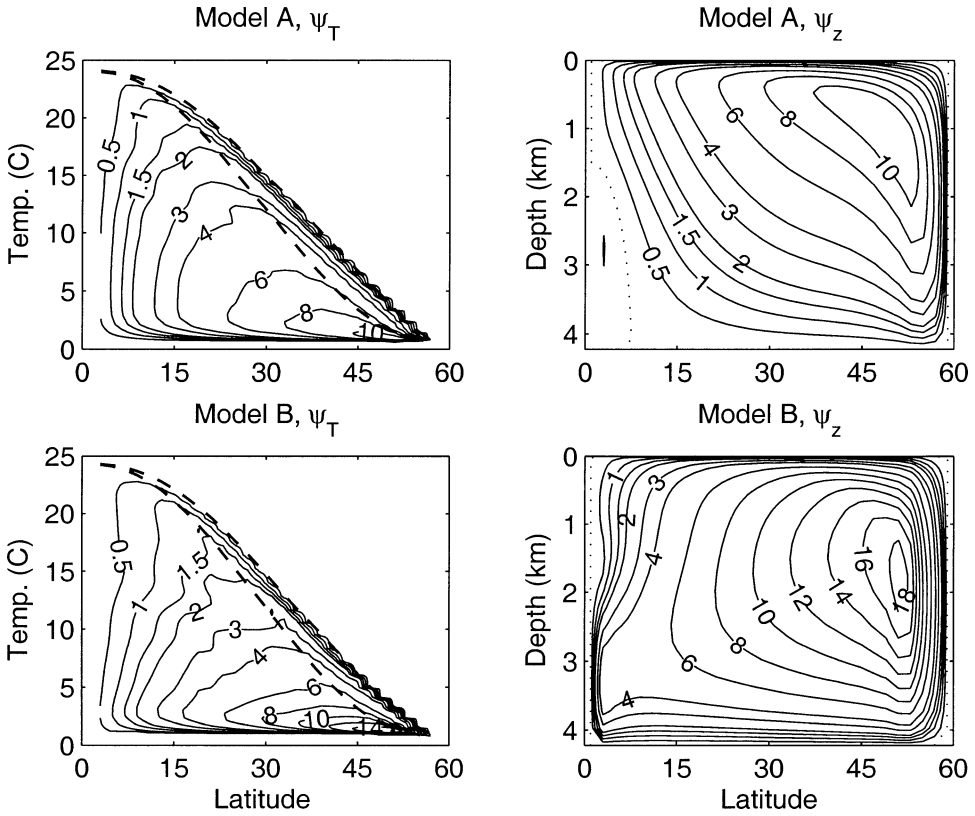

FIG. 1. The meridional overturning in T and z representations [see Eq. (29)] calculated for $\Delta T = 25°C$ (corresponding to $\Delta\rho = 5$ kg m^{-3}) for models (top) A and (bottom) B, respectively. The overturning is measured in units of Sverdrup (Sv $\equiv 10^6$ m^3 s^{-1}). The dashed lines indicate the range of sea surface temperatures as a function of latitude.

sponse to a weaker equator-to-Pole density difference. The relations in Eq. (22c) were presented (in a somewhat different notation) by Huang (1999).

d. Additional remarks

To broaden the discussion, we analyze possible overturning behaviors that follow from diffusivity representation

$$\kappa \propto N^{-q}, \tag{23}$$

where the parameter q controls the dependence of diffusivity on the local buoyancy frequency. By substituting this diffusivity into Eq. (6), we find that $\zeta = q/2$ and $\eta = 1 - q/2$, which [through Eq. (9)] yields

$$\lambda = (2 - 3q)/(6 - q). \tag{24}$$

This formula gives a range of THC behaviors, including some of the cases presented in Table 1. One point that bears discussion is what happens when $q = 2$ (implying $\lambda = -1$). This particular choice leads to a constant vertical buoyancy flux over the entire water column. As a consequence, the surface buoyancy flux would penetrate undiminished to the bottom, and in general it would be impossible to satisfy surface boundary conditions. Under these conditions, the ocean would probably never reach a quasi equilibrium with the atmosphere, which could result in a chaotic climate (as opposed to the earth's present chaotic weather). This dramatic state of affairs indicates that values of q close to 2 must be viewed as fairly unrealistic. It is interesting to note that Huang (1999) implemented a parameterization that corresponds essentially to the case $q = 2$ in an ocean model and reported pronounced time dependence in some of his simulations.[2]

A more interesting case is the one in which $q = 2/3$. This case yields a constant overturning strength as changes in the density difference are exactly compensated by changes in thermocline depth. However, there is no physical peculiarity associated with this behavior, which just marks the transition between the regimes for which the circulation either increases or decreases with density difference.

[2] Huang prescribed the local dissipation according to $\epsilon = e(z)$, where e was some given function; in view of Eq. (11), this leads to $\kappa \propto N^{-2}$. Note that although this parameterization implies a constant $\mathcal{E}$, it does not yield the same overturning dynamics as the case C; see Table 1.

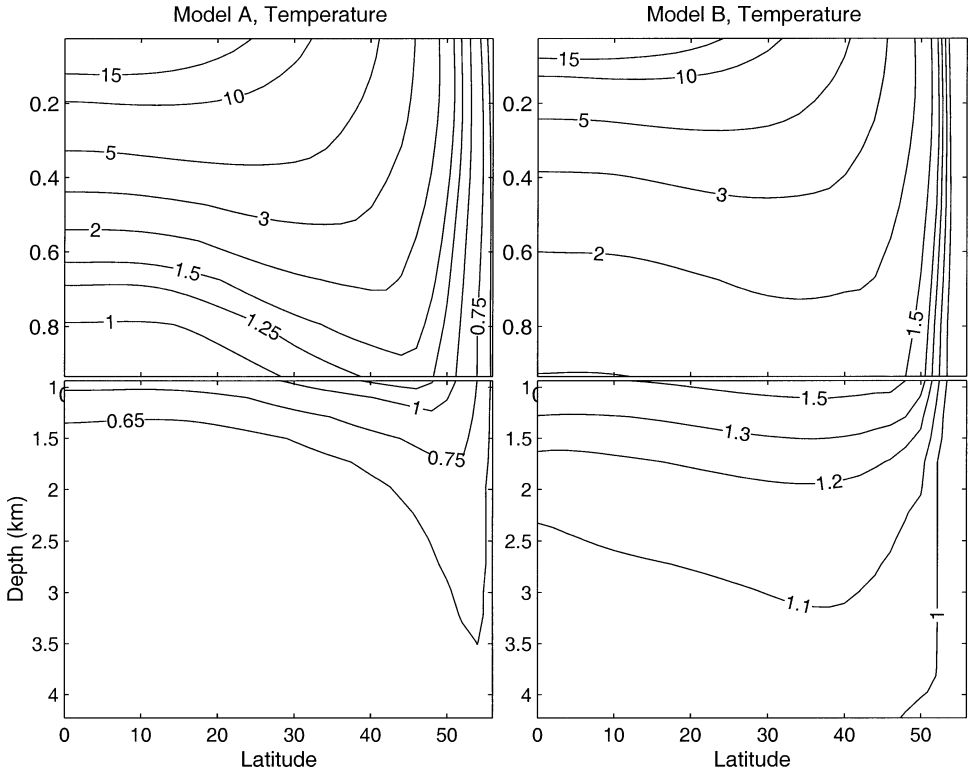

FIG. 2. The zonally averaged temperature distribution simulated for $\Delta T = 25$°C (corresponding to $\Delta\rho = 5$ kg m^{-3}) for models (left) A and (right) B, respectively. For clarity, the upper 1000 m are enlarged. Note that, as in the ocean, the equator-to-Pole temperature difference is virtually equal to the vertical temperature difference in low latitudes.

3. Numerical simulations

To further explore this issue, we have performed a set of simulations with an ocean circulation model. We use the MIT model (Marshall et al. 1997) in a basin of constant depth (4400 m) stretching from the equator to 60° N and extending 40° zonally. The resolution is 2° × 2°, horizontally with 26 vertical levels. Note that the wind forcing is set to zero in all simulations reported here. At the surface, the temperature is relaxed toward the target field

$$T = T_0 + \Delta T[1 + \cos(\pi\phi/\phi_N)]/2, \qquad (25)$$

where ΔT is the north–south temperature difference, ϕ is the latitude, and $\phi_N = 60°$ is the northern boundary. The relaxation timescale is 50 days, which implies that the surface temperature is nearly prescribed in our simulations. The density is a linear function of temperature

$$\rho = \rho_0(1 - \alpha T), \qquad (26)$$

where $\rho_0 = 1000$ kg m^{-3} and $\alpha = 2 \times 10^{-4}$ K^{-1}. The horizontal and vertical eddy viscosities are 5×10^3 and 10^{-3} m^2 s^{-1}, respectively. To avoid spurious diapycnal mixing, due to horizontal diffusion across sloping density surfaces, we employ the GM scheme (Gent and McWilliams 1990). This scheme represents isopycnal mixing of tracers by baroclinic eddies. In all simula-

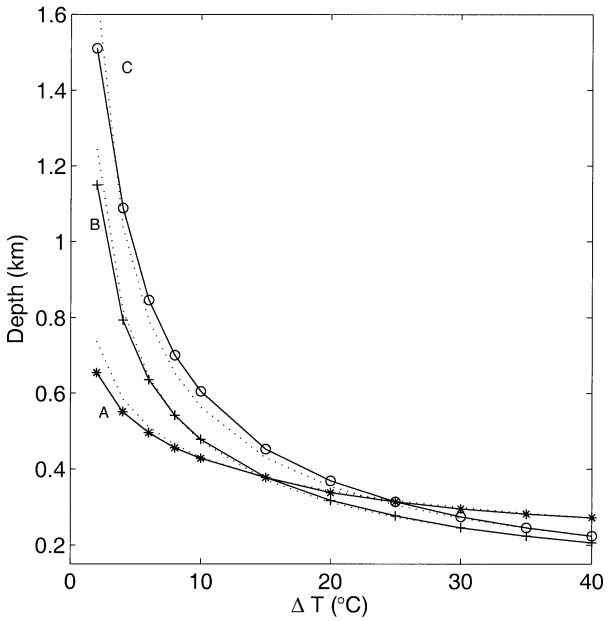

FIG. 3. The thermocline depth at 30° latitude as a function of the equator-to-Pole temperature difference. The thermocline depth is calculated from the model results according to Eq. (30). Stars, plus signs, and circles indicate results obtained with fixed κ (A), with $\kappa \propto N^{-1}$ (B), and with $\kappa \propto \Delta T^{-1}$ (C). The thin dotted lines depict the relation between H and ΔT obtained from the scale analysis; see Eqs. (22a)–(22c).

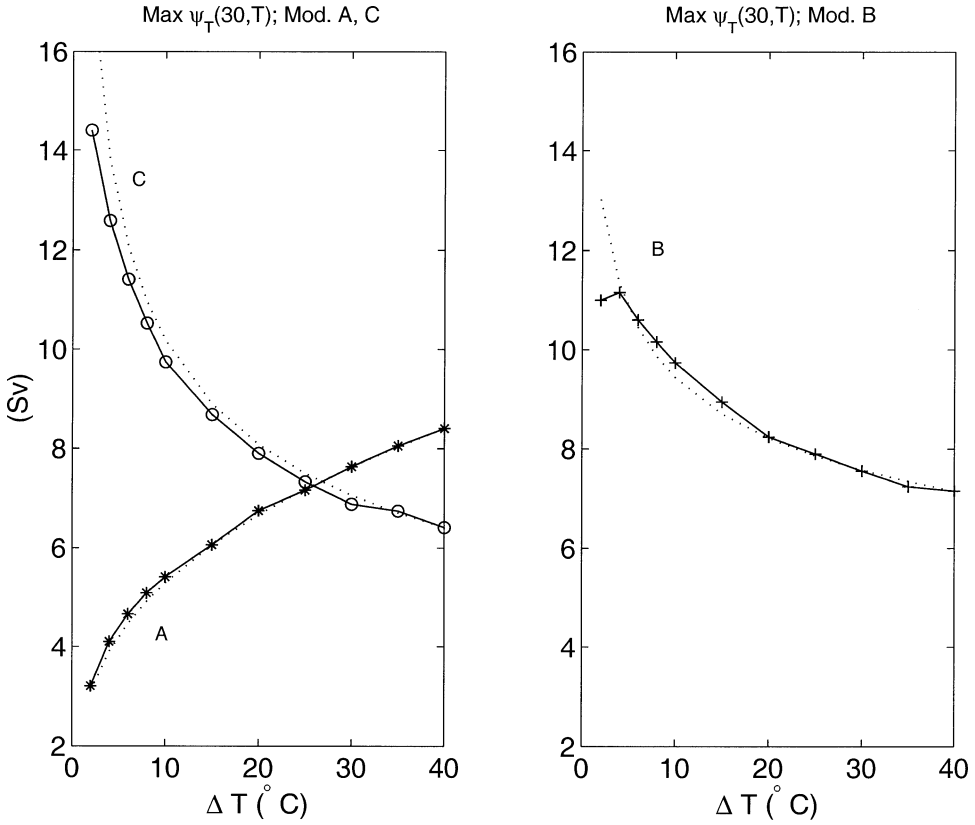

FIG. 4. The overturning strength, measured by the maximum of ψ_T at 30° latitude, as a function of the equator-to-Pole temperature difference. Stars, plus signs, and circles indicate results obtained with models A, B, and C, respectively. (For clarity, the results from model B are shown in the right panel.) The thin dotted lines depict the relation between ψ and ΔT obtained from the scale analysis; see Eqs. (22a)–(22c).

tions, the isopycnal diffusivity is set to $10^3\ \mathrm{m^2\ s^{-1}}$. Three representations of the vertical diffusivity are considered.

Model A: constant diffusivity; $\kappa = 10^{-4}\ \mathrm{m^2\ s^{-1}}$.

Model B: a stability-dependent diffusivity of the form (e.g., Gargett 1984)

$$\kappa = a_0 N^{-1}, \tag{27}$$

with $a_0 = 7 \times 10^{-7}\ \mathrm{m^2\ s^{-2}}$. In this case, we have imposed an upper bound on κ (i.e., $10^{-2}\ \mathrm{m^2\ s^{-1}}$).

Model C: constant mixing energy and spatially uniform diffusivity. This case is implemented as

$$\kappa = \kappa_0(\Delta T_0/\Delta T), \tag{28}$$

where $\kappa_0 = 10^{-4}\ \mathrm{m^2\ s^{-1}}$, ΔT is the imposed equator-to-Pole temperature contrast, and $\Delta T_0 = 25$°C. This formula keeps the spatially integrated production of potential energy due to vertical diffusion [see Eq. (16)] essentially fixed. Note further that, when the imposed surface temperature difference ΔT is equal to 25°C, models A and C yield identical results.

a. Representations of the overturning

We are interested in to what extent the scale analysis captures the overturning strength simulated by the model. A general streamfunction of the meridional overturning can be defined as (Hirst et al. 1996)

$$\psi_\xi(y, \xi) = \int\int_{z(x,y,\xi)}^{0} v(x, y, z')\, dx\, dz', \tag{29}$$

where $\xi(x, y, z)$ is a scalar field and x and y denote the zonal and meridional coordinates, respectively. (Note that when we compute ψ, v is the Eulerian velocity; the bolus GM velocity is disregarded, because it is quite weak in our simulations.) When $\xi = z$, we obtain the standard streamfunction in the height coordinates, where $\psi_z(y, z)$ measures the northward transport between the surface and the depth z. Alternatively, the meridional overturning may be represented in density coordinates. An advantage with this representation is that the streamfunction $\psi_\rho(y, \rho)$ measures the true diapycnal transport, that is, showing the actual watermass transformation. In situations where the isopycnal surfaces slope in the east–

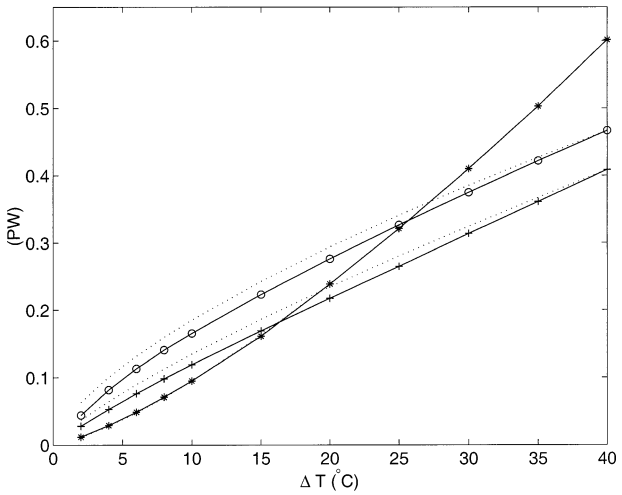

FIG. 5. The maximum poleward heat flux (advective plus diffusive) as a function of the equator-to-Pole temperature difference. The heat flux (given in units of petawatt, 1 PW = 10^{15} W) peaks near 30° latitude and is dominated by its advective component. Stars, plus signs, and circles indicate results from models A, B, and C, respectively. The dotted lines indicate the theoretical estimates of the heat flux; see the text.

west direction, ψ_ρ and ψ_z may give very different pictures of the overturning.[3]

Because we use a linear equation of state and specify the target pole-to-equator temperature difference, it is convenient to calculate the overturning using the temperature as the measure of density. In what follows, we will thus consider ψ_T rather than ψ_ρ.

b. The structure of the overturning

The three versions of the model, which differ only in the representation of κ, are run to steady states for increasing values of ΔT. Figure 1 shows the meridional overturning streamfunction (ψ_z and ψ_T) obtained for $\Delta T = 25$°C. (Note that, since models A and C are designed to be identical at $\Delta T = 25$°C, model C is not shown.) In height coordinates, the overturning is stronger and has a deeper structure in model B, reflecting that κ increases in the weakly stratified deep ocean. When comparing the two simulations, it is important to recognize that, at $\Delta T = 25$°C, the global mean κ is about 10 times as large in model B as it is in model A. (The thermocline κ values are comparable, but model B yields κ values on the order of 10^{-3} m^2 s^{-1} at greater depths.) Thus, the overturning amplitudes are not directly comparable, and one should primarily contrast the different flow structures in the two models.

As illustrated in Fig. 2, the corresponding temperature distributions appear more similar; the elevated deep-water temperature in model B is perhaps the most conspicuous difference. A closer inspection reveal that both mixing representations produce similar stratifications in the upper thermocline, where N is on the order of 10^{-2} s^{-1}. However, the simulated lower thermocline and deep ocean stratifications are generally too weak to match observations. These structural differences have been discussed in detail by Cummins et al. (1990). [See Hirst and Cai (1994) for a discussion on the effects of introducing the parameterization $\kappa \propto N^{-1}$ in a World Ocean model.]

c. The overturning response

The main objective here is to explore how the representation of κ affects the *response* of the THC to changes in the equator-to-Pole density difference—rather than the structural changes attributable to different spatial distributions of κ. Consider first the response of the thermocline depth, which is quantified with a thermocline depth index defined as

$$H_T = \int_{-D}^{0} T^*(z)\, dz. \tag{30}$$

Here, D is the depth of the basin and T^* is a nondimensional representation of the zonally averaged temperature at 30° latitude:

$$T^*(z) = \frac{T(z) - T(z = -D)}{T(z = 0) - T(z = -D)}. \tag{31}$$

Figure 3 illustrates the dependence of H_T on the imposed surface temperature difference. The result from the scale analysis is also shown, demonstrating a close similarity with the result from the numerical simulations; see Eqs. (22a)–(22c). Note that the relations between H_T and ΔT diagnosed at 30° latitude are representative for the southern two-thirds of the models, where a well-defined thermocline is encountered. As predicted by the scale analysis, the changes in thermocline depth are greater in model B and C than in model A. According to the theoretical considerations, this higher sensitivity of the thermocline depth should yield an overturning that decreases rather than increases with increasing ΔT in model B and C.

To analyze whether this prediction is reproduced in the numerical simulations, we have calculated the maximum of the overturning in temperature coordinates ψ_T at 30° latitude; see Eq. (29). As shown in Fig. 4, the simulated responses of ψ_T agree reasonably with the theoretical predictions. In agreement with previous investigations [see Park and Bryan (2000) for a review], the model with a uniform fixed κ yields an overturning that increases with increasing density difference. In contrast, the stratification dependent κ representations (models B and C), yield overturning strengths that tend to decrease with increasing density difference. It is worth iterating that in models B and C, a decrease in

[3] One prominent example is the Deacon cell in the Southern Ocean, where the diapycnal overturning (ψ_ρ) is small in comparison with the overturning measured by ψ_z (e.g., Döös and Webb 1994).

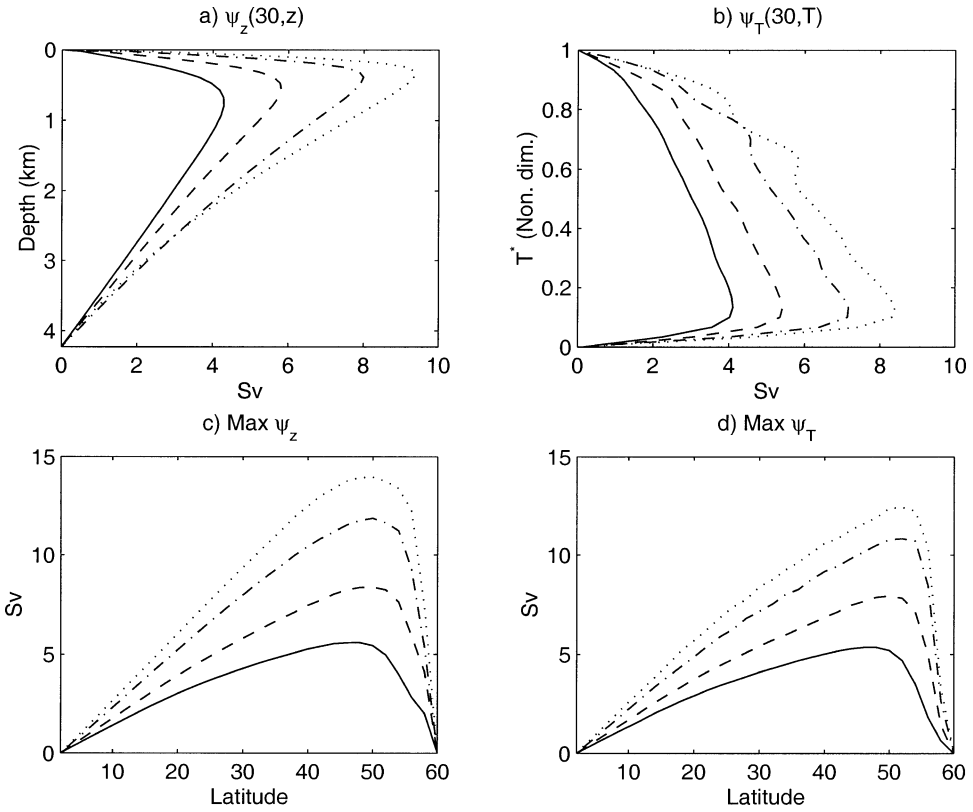

FIG. 6. Model A (constant κ): Views of the overturning for different equator-to-Pole temperature differences (solid line $\Delta T = 4$°C, dashed line $\Delta T = 10$°C, dash-dotted line $\Delta T = 25$°C, dotted line $\Delta T = 40$°C): overturning in (a) z coordinates and (b) T coordinates at 30° latitude. Note that $T^* = (T - T_{\min})/(T_{\max} - T_{\min})$, where the max and mean values refer to the temperature field at 30° latitude. Maximum (c) of ψ_z and (d) of ψ_T as a function of latitude.

the imposed density difference results in an increase of the diffusivity. The enhanced vertical mixing deepens the thermocline, which in turn acts to strengthen the overturning; see Eq. (3). If this increase in vertical mixing is sufficiently strong, the overturning amplifies even though the equator-to-Pole density difference diminishes. In conclusion, the scale analysis must be viewed as successful in predicting how the representation of κ affects the qualitative dependence of the thermocline depth H_T and ψ_T on ΔT.

Because the poleward heat flux in the ocean is of immediate importance for the climate, it is of interest to analyze how the quantity is influenced by the properties of κ. A straightforward estimate of the advective component of the poleward heat flux is given by $\psi\Delta T$. Accordingly, the scale analysis suggests that heat flux should be proportional to $\Delta T^{4/3}$, $\Delta T^{4/5}$, and $\Delta T^{2/3}$, respectively, in cases A, B and C. Figure 5 shows the simulated maximum heat flux (encountered near 30° latitude in all three models) as a function of ΔT. As illustrated, the simulated heat flux very closely follows the theoretical prediction in model A, whereas the correspondence between theory and simulations is only qualitative in model B and C.

It deserves to be repeated that wind forcing is excluded in the simulations presented here. Thus, it is relevant to report that some preliminary numerical investigations indicate that the present results also hold true qualitatively when a constant wind forcing is applied. However, to explore the combined effects of wind forcing and mixing is beyond the scope of this paper, and the reader is referred to the studies of Samelson and Vallis (1997) and Vallis (2000) for some scaling results pertinent to wind-forced circulation.

d. How well does model B follow the scale theory?

As illustrated in Fig. 4, the simulated response of ψ_T at 30° latitude follows qualitatively the results of the scale analysis. It is relevant to ask whether this overturning index is representative for the whole model domain and how it compares with the response of the overturning in z coordinates ψ_z. The short answer is that in models A and C, ψ_T at 30° latitude essentially mirrors the global response of ψ_T as well as ψ_z. In model B, on the other hand, there are features of the overturning response that warrant further discussion. Figures 6–8 show the spatial distribution of the response of ψ_T and

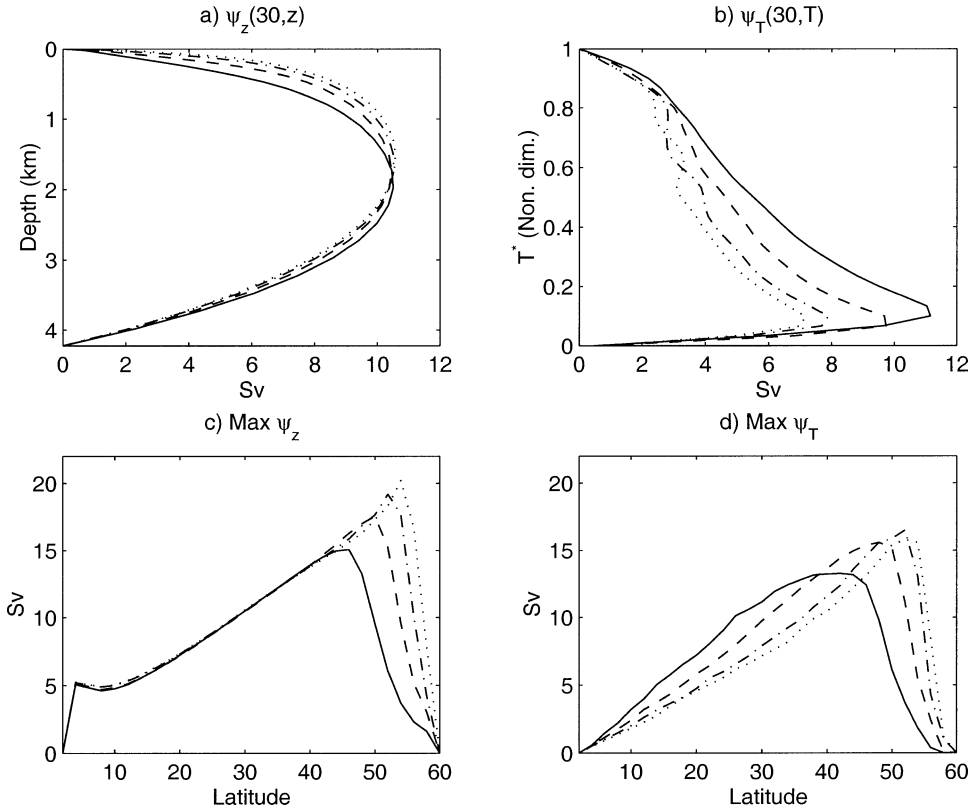

FIG. 7. Same as in Fig. 6 but for model B (with $\kappa \propto N^{-1}$). Note the difference in the (d) response of ψ_T north and south of 40° latitude.

ψ_z in the three models. In model A, details are straightforward: a greater density contrast yields an overall amplification of the overturning. Regardless of whether low or high latitudes are considered, the indices ψ_T and ψ_z follow closely the predicted $\Delta\rho^{1/3}$ dependence. As illustrated in Fig. 7, the response of the overturning in the model B is more complicated. At 30° latitude, ψ_T shows an overall decrease with increasing density, while the maximum of ψ_z is virtually independent of the surface density difference; see also Fig. 10. Furthermore, poleward of 40° where the overturning reaches its maximum, ψ_T increases weakly with increasing density contrast. In model C, the responses of ψ_T and ψ_z are again similar, following roughly the predicted $\Delta\rho^{-1/3}$ dependence. The exception is the very high latitudes where the overturning intensifies with $\Delta\rho$.

It is not entirely surprising that the high-latitude response of ψ in models B and C deviates from the scale relations in Eqs. (22b) and (22c). In the northern model domain, strong recirculation is encountered and the weak stratification is no longer governed by the advective–diffusive balance [Eq. (2)]. Rather, convection and lateral eddy diffusion in the deep mixed layers become important in the buoyancy budget (Marshall et al. 1999). Here, east–west and vertical density differences are comparable, indicating that the depth scale of the stratification is essentially set by the basin depth. Accordingly, the the thermocline adjustment mechanism, active in low latitudes, should play a limited role in high latitudes. In fact, if the stratification depth scale is fixed by the basin depth, the thermal wind balance [Eq. (1)] suggests that the overturning strength should essentially be proportional to $\Delta\rho$. (Note that, although the vertical diffusivity becomes large in the weakly stratified region in model B, the imposed upper bound on κ is not reached, except in a few grid cells on the northern boundary. Thus, the high-latitude response of ψ should not be attributable to a saturation of κ at its constant upper value.)

Let us now turn to the different low-latitude responses of ψ_T and ψ_z in model B. In essence, we believe that

1) the response of ψ_T reflects the changes in thermocline depth emphasized in the scale analysis and
2) the maximum of ψ_z, which is encountered well below the thermocline at middepths, is primarily controlled by the stratification in the deep ocean—a dynamical feature not considered in the scale analysis.

This view is based on the following considerations: Focus to begin with on Fig. 9, which illustrates the meridional velocity distribution at 30° latitude as simulated by models A and B for $\Delta T = 25$°C. In the figure, the

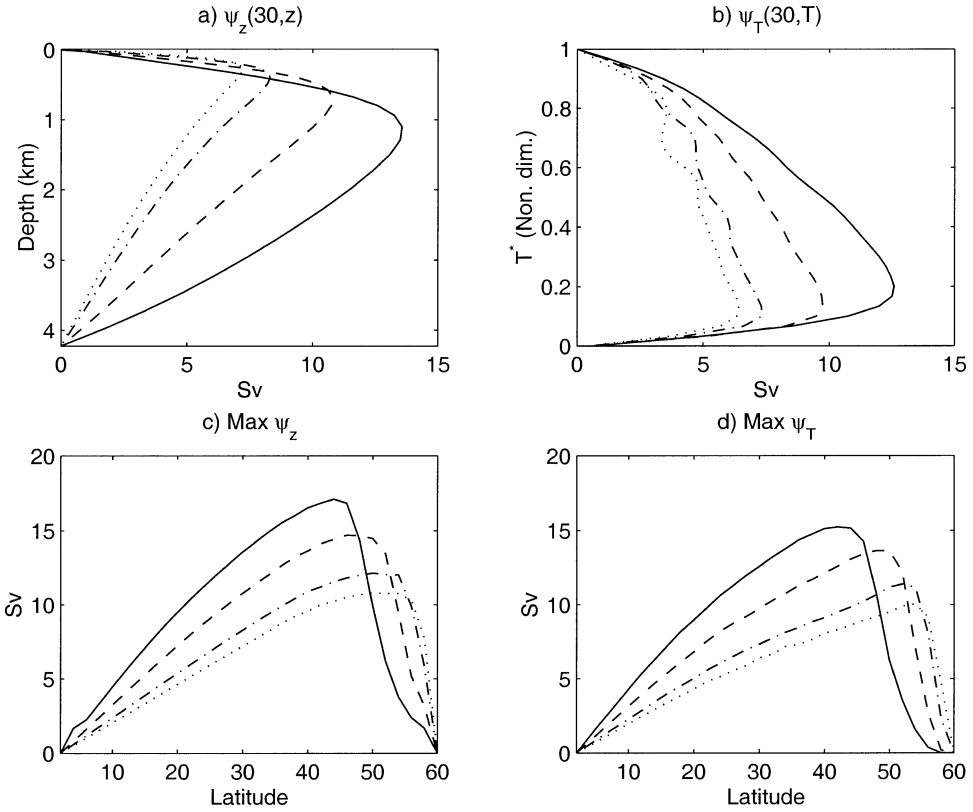

FIG. 8. As in Fig. 6 but for model C (with $\kappa \propto \Delta T^{-1}$).

locations of a few selected isotherms as well as the isotherm corresponding to the maximum of ψ_T are shown. The latter isotherm distinguishes between warm (cold) temperature classes associated with net poleward (equatorward) transport. As shown in Fig. 9, the net transport of water between any two isotherms warmer than about 2.5°C is directed poleward in model A as well as in model B. Thus, the net *diapycnal* upwelling south of 30° reaches its maximum on the 2.5°C isotherm in both models. An inspection of Fig. 2 reveals that this isotherm is encountered around a depth of 600 m. In model A, the net upwelling in height coordinates also attains its maximum in that depth range; see Fig. 6. In model B, on the other hand, $\psi_z(30, z)$ peaks nearly 1500 m deeper, at a depth close to 2000 m. Moreover, the maximum of ψ_z is greater than the maximum of ψ_T, indicating that ψ_z captures a considerable amount of recirculation on constant density surface in model B; see Fig. 10. Accordingly, we believe that the maximum of ψ_T is the relevant index to compare with the scale theory that, although formulated in height coordinates, pertains to diapycnal upwelling. This view is further corroborated by the fact that ψ_T attains its maximum in the thermocline region and that thermocline depth response roughly obeys the simple scaling law.

Having said this, it is fair to emphasize that the abyssal east–west density gradients and the associated vigorous deep circulation in model B are a significant dynamical feature that is not accounted for in the simple scale considerations. The increase in diffusivity with depth implied by the $\kappa \propto N^{-1}$ parameterization certainly plays an important role for energizing the abyssal flow. We believe, however, that the deep circulation to some extent is decoupled from the diapycnal thermocline circulation in model B. This view is supported by the result of simulations with a model that is identical to model B except from that the basin depth is reduced from 4400 to 2800 m. (The shallow model has 20 vertical grid points, whereas the original has 26. The stratifications in the two models are essentially similar and not further discussed here.) As illustrated in Fig. 10, the maximums of $\psi_T(30, T)$ are essentially equal in the shallow and the deep basin when ΔT exceeds 15°C. In contrast, the maximum of $\psi_z(30, z)$ in the shallow basin (encountered around 1000 m) is systematically weaker than in the deep basin. This indicates that the strength of the deep circulation is directly influenced by basin depth when the diffusivity obeys $\kappa \propto N^{-1}$. For a given basin depth, on the other hand, the strength of the abyssal circulation is remarkably insensitive to the imposed surface density difference. However, we will not here further explore the dynamics of the abyssal circulation in model B, because this issue is outside the main focus of the present study.

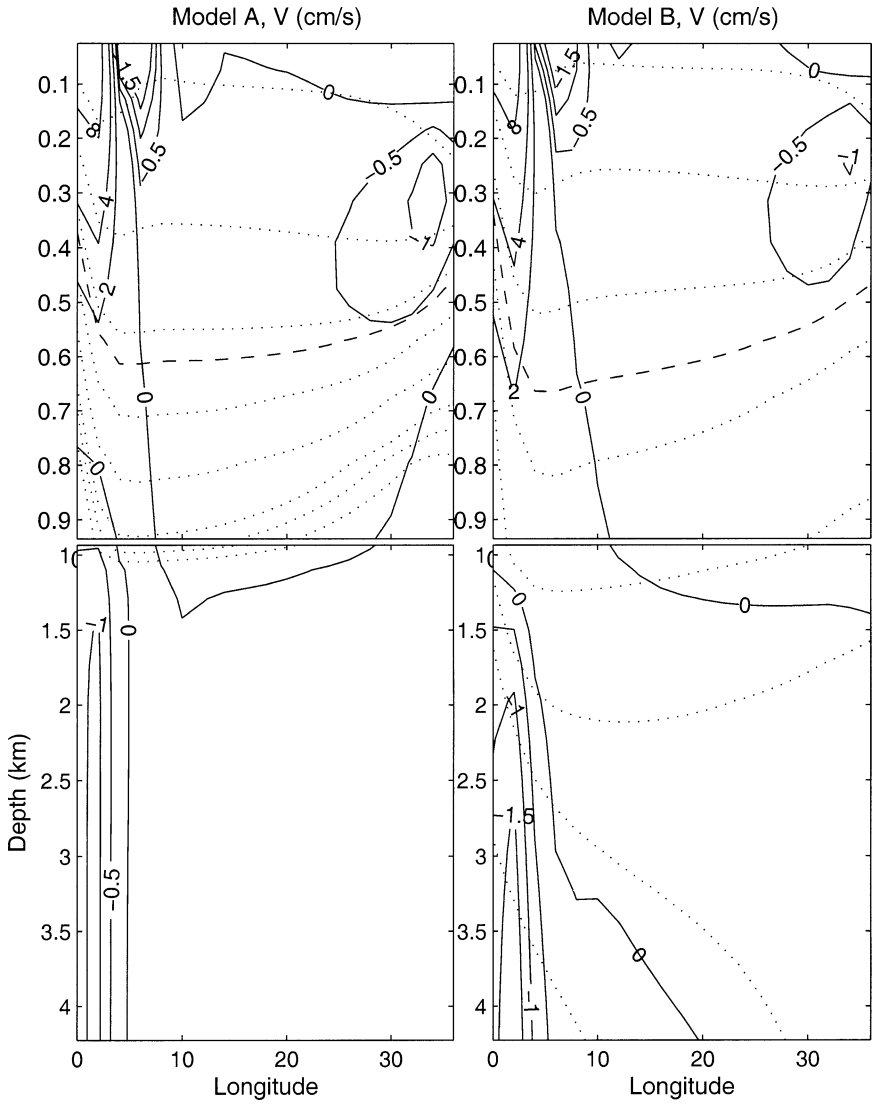

FIG. 9. Meridional velocity at 30° latitude obtained for $\Delta T = 25$°C. The dotted lines indicate the isotherms 1°, 1.1°, 1.2°, 1.5°, 2°, 3°, 5°, and 10°C. The dashed line is the isotherm for which $\psi_T(30, T)$ attains its maximum value; above (below) this isotherm the net meridional transport is directed poleward (equatorward).

e. The limit of weak density differences

A concluding point that deserves a comment is what happens when the surface density contrast becomes very weak. In this limit, the scale analysis predicts that the overturning in models B and C should grow beyond bounds; see Table 1. Obviously, some neglected effect will eventually limit the overturning. As it turns out, one assumption in the thermocline scaling breaks down when $\Delta\rho$ become very small: the requirement that the thermocline depth (H) must be much smaller than the depth of the ocean (e.g., Park and Bryan 2000). As illustrated in Fig. 3, a reduced density contrast is associated with a greater thermocline depth in all three model configurations. Hence, for sufficiently weak density contrast, the depth scale of the stratification will become comparable to the basin depth. As this occurs, the thermocline depth cannot increase further and, in view of Eq. (3), we expect that the overturning should be proportional to $\Delta\rho$— regardless of the representation of κ. (Recall that we have already invoked this effect as a possible explanation for behavior of the high-latitude overturning in model B.)

It is presumably the finite basin depths that cause the downward trend in the overturning that is seen for small values of ΔT in Fig. 10. The fact that the maximum of ψ_T is essentially independent of the basin depth for large density differences supports this straightforward interpretation. Accordingly, the ocean depth imposes a limit on how much the THC can be intensified, through enhanced mixing, in response to a decreasing equator-to-Pole density difference.

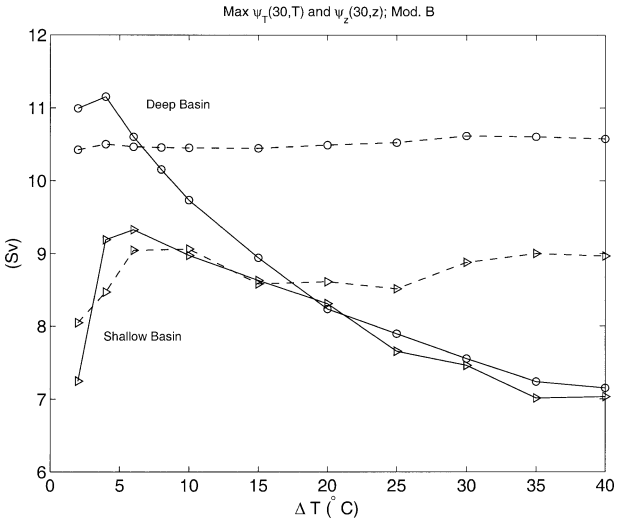

FIG. 10. The maximums of ψ_T (solid lines) and ψ_z (dashed lines) at 30° latitude simulated with model B, where $\kappa \propto N^{-1}$. Circles indicate results from the standard version of the model, which has a basin depth of 4400 m, and triangles indicate results from simulations in which the basin depth is reduced to 2800 m.

4. Discussion

Our main result is that the THC may intensify, rather than slow down, in response to a reduced equator-to-Pole density difference. This unconventional state of affairs—that a stronger density difference yields a weaker overturning—occurs in our one-hemisphere ocean model when the stratification-dependent diffusivity parameterizations in Eqs. (27) and (28) are employed. Based on the theoretical considerations in section 2, we believe that a rather wide class of stability-dependent mixing schemes would yield the ''reversed'' THC dynamics simulated here. This view is supported by the numerical simulations of Huang (1999), who employed another stability-dependent diffusivity representation ($\kappa \sim N^{-2}$, roughly) and found that the overturning in his one-hemisphere model intensified when the density contrast was reduced.

It must be underlined that exploring and parameterizing the oceanic mixing is an active research field (e.g., Toole and McDougall 2001). The results of this study, which indicate that the physics of small-scale vertical mixing could strongly influence the response of the THC to changes in surface fluxes of heat and freshwater, highlight the importance of further observational and theoretical studies of vertical mixing. For the sake of the argument, however, let us suppose that the properties of the vertical mixing in the World Ocean imply that the low-latitude upwelling would be enhanced in response to a reduced equator-to-Pole density difference. Would this increase in low-latitude upwelling also yield a stronger meridional overturning? In a one-hemisphere basin (as our model), this is by necessity the case because the high-latitude sinking must balance the low-latitude upwelling. In the ocean, on the other hand, the response of the wind-driven upwelling in the Southern Ocean has to be taken into account. Clearly, if the Southern Ocean upwelling is fixed, then a weaker density difference would be associated with stronger overturning.[4]

To elaborate the argument, it is necessary to consider the effect of baroclinic eddies, which may play a role in controlling the upwelling in the Southern Ocean (e.g., Gnanadesikan 1999; Karsten et al. 2002). Essentially, the eddies in the circumpolar Southern Ocean induce a southward mass flux that partly cancels the northward Ekman transport. As demonstrated in the eddy-resolving simulations of Karsten et al. (2002), the eddy-induced mass transport depends on the surface density gradient as well as on the thermocline depth. Thus, a change in the equator-to-Pole density difference is expected to affect both the low-latitude upwelling and the Southern Ocean eddy transport; however, it is beyond the scope of the present work to further address this issue.

Keeping in mind that the relevance of our results for the real ocean needs to be further investigated, we point out an intriguing possibility concerning the impact of freshwater forcing on the THC. The freshwater forcing resulting from the poleward flow of moisture in the atmosphere creates a salinity field that reduces the thermally imposed density contrast between equatorial and polar surface waters. As a result, the stratification of the water column in subtropical and tropical waters becomes weaker. If the mixing intensity depends on stratification, it is possible that the THC is amplified rather than curtailed by the freshwater forcing. Thus, a warmer climate associated with a stronger freshwater forcing will not necessarily imply a curtailed THC. Rather, an amplification could be expected.

An amplification from the freshwater forcing on the THC may contribute to explain the much warmer climates that have occurred on the earth. Lyle (1997), for instance, has proposed that the weak equator-to-Pole temperature difference during the early Cenozoic (some 60–40 million years ago) could have sustained itself through a positive feedback on the THC resulting from enhanced vertical mixing. Including also the freshwater forcing in the feedback mechanism may strengthen this hypothesis (Nilsson and Walin 2001). Although speculative, we believe that this is a geophysically interesting issue that certainly warrants further investigations.

Acknowledgments. We are grateful for the constructive and insightful comments provided by Dr. Jeffery R. Scott and three anonymous reviewers, which lead to significant improvements of the original manuscript. One reviewer generously outlined the discussion on internal wave dissipation and vertical diffusivity in section

[4] Regardless of the features of κ, however, the sensitivity of the overturning on $\Delta\rho$ should be weaker as the wind supplies a fixed upwelling contribution (see, e.g., the conceptual model of Gnanadesikan 1999).

2. This work was supported by the Swedish Science Research Council and by MISTRA through the SWECLIM programme. Further, we thank the Knut and Alice Wallenberg Foundation, which financed the Linux cluster ''Otto'' on which the simulations were performed, and the staff at the National Center for Super Computing in Linköping for their technical assistance.

REFERENCES

Bell, T. H., 1975: Topographically generated internal waves in the open ocean. *J. Geophys. Res.,* **80,** 320–327.

Broecker, W. S., 1997: Thermohaline circulation, the achilles heel of our climate system: Will man-made CO_2 upset the current balance? *Science,* **278,** 1582–1588.

Bryan, K., and L. J. Lewis, 1979: A water mass model of the World Ocean. *J. Geophys. Res.,* **84,** 2503–2517.

Cummins, P. F., G. Holloway, and A. E. Gargett, 1990: Sensitivity of the GFDL ocean general circulation model to a parameterization of vertical diffusion. *J. Phys. Oceanogr.,* **20,** 817–830.

Döös, K., and D. J. Webb, 1994: The Deacon cell and the other meridional cells of the Southern Ocean. *J. Phys. Oceanogr.,* **24,** 429–442.

Emanuel, K., 2001: Contribution of tropical cyclones to meridional heat transport by the oceans. *J. Geophys. Res.,* **106** (D14), 14 771–14 781.

Gargett, A. E., 1984: Vertical eddy diffusivity in the ocean interior. *J. Mar. Res.,* **42,** 359–393.

——, and G. Holloway, 1984: Dissipation and diffusion by internal wave breaking. *J. Mar. Res.,* **42,** 15–27.

Gent, P. R., and J. C. McWilliams, 1990: Isopycnal mixing in ocean circulation models. *J. Phys. Oceanogr.,* **20,** 150–155.

Gnanadesikan, A., 1999: A simple predictive model for the structure of the oceanic pycnocline. *Science,* **283,** 2077–2079.

Hirst, A. C., and W. J. Cai, 1994: Sensitivity of a World Ocean GCM to changes in subsurface mixing parameterizations. *J. Phys. Oceanogr.,* **24,** 1256–1279.

——, D. R. Jackett, and T. J. McDougall, 1996: The meridional overturning cells of a World Ocean model in neutral coordinates. *J. Phys. Oceanogr.,* **26,** 775–791.

Huang, R. X., 1999: Mixing and energetics of the oceanic thermohaline circulation. *J. Phys. Oceanogr.,* **29,** 727–746.

Karsten, R., H. Jones, and J. Marshall, 2002: The role of eddy transfer in setting the stratification and transport of a circumpolar current. *J. Phys. Oceanogr.,* **32,** 39–54.

Ledwell, J. R., E. T. Montgomery, K. L. Polzin, L. C. Laurent, R. W. Schmitt, and J. M. Toole, 2000: Evidence for enhanced mixing over rough topography in the abyssal ocean. *Nature,* **403,** 179–182.

Llewellyn-Smith, S. G., and W. R. Young, 2002: Conversion of the baroropic tide. *J. Phys. Oceanogr.,* **32,** 1554–1566.

Lyle, M., 1997: Cloud early Cenozoic thermohaline circulation have warmed the poles? *Paleoceanography,* **12,** 161–167.

Marotzke, J., 1997: Boundary mixing and the dynamics of three-dimensional thermohaline circulations. *J. Phys. Oceanogr.,* **27,** 1713–1728.

——, 2000: Abrupt climate change and the thermohaline circulation: Mechanisms and predictability. *Proc. Natl. Acad. Sci. USA,* **97,** 1347–1350.

——, and J. R. Scott, 1999: Convective mixing and the thermohaline circulation. *J. Phys. Oceanogr.,* **29,** 2962–2970.

Marshall, J., C. Hill, L. Perleman, and A. Adcroft, 1997: Hydrostatic, quasi-hydrostatic, and non-hydrostatic ocean modeling. *J. Geophys. Res.,* **102** (C3), 5733–5752.

——, D. Jamous, and J. Nilsson, 1999: Reconciling thermodynamic and dynamic methods of computation of water-mass transformation rates. *Deep-Sea Res.,* **46,** 545–572.

McComas, C. H., and P. Müller, 1981: Time scales of resonant interaction among oceanic internal waves. *J. Phys. Oceanogr.,* **11,** 139–147.

Munk, W. H., and C. Wunsch, 1998: Abyssal recipes II: Energetics of tidal and wind mixing. *Deep-Sea Res.,* **45A,** 1977–2010.

Nilsson, J., 1996: Mixing in the ocean produced by tropical cyclones. *Tellus,* **48A,** 342–355.

——, and G. Walin, 2001: Freshwater forcing as a booster of thermohaline circulation. *Tellus,* **53A,** 628–640.

Osborne, T. R., 1980: Estimates of the local rate of vertical diffusion from dissipation measurements. *J. Phys. Oceanogr.,* **10,** 83–89.

Park, Y.-G., and K. Bryan, 2000: Comparison of thermally driven circulation from a depth-coordinate model and an isopycnal model. Part I: Scaling-law sensitivity to vertical diffusivity. *J. Phys. Oceanogr.,* **30,** 590–605.

Polzin, K. L., J. M. Toole, and R. W. Schmitt, 1995: Finescale parameterizations of turbulent dissipation. *J. Phys. Oceanogr.,* **25,** 306–328.

——, ——, J. R. Ledwell, and R. W. Schmitt, 1997: Spatial variability of turbulent mixing in the abyssal ocean. *Science,* **276,** 93–96.

Rahmstorf, S., 2000: The thermohaline ocean circulation: A system with dangerous thresholds? *Climatic Change,* **46,** 247–256.

Samelson, R. M., and G. K. Vallis, 1997: Large-scale circulation with small diapycnal diffusion: The two-thermocline limit. *J. Mar. Res.,* **55,** 223–275.

Sjöberg, B., and A. Stigebrandt, 1992: Computations of the geographical distribution of the energy flux to mixing processes via internal tides and the associated vertical circulation in the ocean. *Deep-Sea Res.,* **39,** 269–291.

Stigebrandt, A., 1987: A model for the vertical circulation of the Baltic deep water. *J. Phys. Oceanogr.,* **17,** 1772–1785.

Toggweiler, J. R., and B. Samuels, 1995: Effect of Drake Passage on the global thermohaline circulation. *Deep-Sea Res.,* **42,** 477–500.

Toole, J., and T. J. McDougall, 2001: Stirring and mixing in the ocean interior. *Ocean Circulation and Climate,* G. Siedler, J. Church, and J. Gould, Eds., Academic Press, 337–356.

Vallis, G. K., 2000: Large-scale circulation and production of stratification: Effects of wind, geometry, and diffusion. *J. Phys. Oceanogr.,* **30,** 933–954.

Webb, D. J., and N. Suginohara, 2001: Vertical mixing in the ocean. *Nature,* **409,** 37.

Welander, P., 1986: Thermohaline effects in the ocean circulation and related simple models. *Large-Scale Transport Processes in the Oceans and Atmosphere,* J. Willebrand and D. L. T. Anderson, Eds., D. Reidel, 163–200.

Weyl, P. K., 1968: The role of the oceans in climate change: A theory of the ice ages. *Causes of Climatic Change, Meteor. Monogr.,* No. 30, Amer. Meteor. Soc., 37–62.

Winters, K. B., and E. A. D'Asaro, 1997: Direct simulation of internal wave energy transfer. *J. Phys. Oceanogr.,* **27,** 1937–1945.